

## PAPER • OPEN ACCESS

# Scanning electron irradiation of hexagonal boron nitride: an efficient procedure for quenching undesired defects emissions monitored by *in-situ* room temperature cathodoluminescence

To cite this article: F Bianco *et al* 2025 *2D Mater.* **12** 025026

View the [article online](#) for updates and enhancements.

## You may also like

- [Surface versus bulk: behavior of photoexcited charge carriers in GeS](#)  
Sepideh Khanmohammadi, Kateryna Kushnir Friedman, Catherine Tran et al.
- [Valley emission and upconversion in isotopically engineered monolayer WS<sub>2</sub> under resonant excitation](#)  
Rahul Kesarwani, Vaibhav Varade, Artur Slobodeniuk et al.
- [Ionically gated transistors based on two-dimensional materials for neuromorphic computing](#)  
Ke Xu and Susan K Fullerton-Shirey



## PAPER

## OPEN ACCESS

RECEIVED  
28 January 2025REVISED  
12 February 2025ACCEPTED FOR PUBLICATION  
10 March 2025PUBLISHED  
26 March 2025

Original content from  
this work may be used  
under the terms of the  
[Creative Commons  
Attribution 4.0 licence](#).

Any further distribution  
of this work must  
maintain attribution to  
the author(s) and the title  
of the work, journal  
citation and DOI.



# Scanning electron irradiation of hexagonal boron nitride: an efficient procedure for quenching undesired defects emissions monitored by *in-situ* room temperature cathodoluminescence

F Bianco<sup>1</sup> , S Pezzini<sup>1</sup> , K Watanabe<sup>2</sup> , T Taniguchi<sup>3</sup> and F Fabbri<sup>1,\*</sup> <sup>1</sup> NEST, Istituto Nanoscienze—CNR, Scuola Normale Superiore, Piazza San Silvestro 12, 56127 Pisa, Italy<sup>2</sup> Research Center for Electronic and Optical Materials, National Institute for Materials Science, 1-1 Namiki, Tsukuba 305-0044, Japan<sup>3</sup> Research Center for Materials Nanoarchitectonics, National Institute for Materials Science, 1-1 Namiki, Tsukuba 305-0044, Japan

\* Author to whom any correspondence should be addressed.

E-mail: [filippo.fabbri@nano.cnr.it](mailto:filippo.fabbri@nano.cnr.it)**Keywords:** hexagonal boron nitride, *in-situ* cathodoluminescence, emission quenching, deep level emissionSupplementary material for this article is available [online](#)

## Abstract

Recently, layered materials have become an interesting platform for quantum optics and nanophotonics. Among them, hexagonal boron nitride (hBN) has attracted a widespread interest due to its peculiar defect-related luminescence properties. In particular, the possible generation and tailoring of color centers by particle irradiation are becoming pivotal aspects for next generation quantum optics and photonics. In this work, we use *in-situ* cathodoluminescence hyperspectral analysis to investigate the effect of fast-scanning, low-voltage electron irradiation on deep level emissions in the ultraviolet (UV) range. The quenching of the UV band (UVB) and changes in the width of the near-band-edge UV luminescence of hBN are investigated as a function of the irradiation time. This quenching is assigned to the electron beam dissociation of in-plane carbon dimer, responsible for such emission, with a concurrent substitutional carbon atoms reconfiguration in donor acceptor pair with a spatial separation in the hBN lattice, that can be optically inactive or can emit in a different optical range, as demonstrated by the intensity decrease of below-bandgap excitation photoluminescence emissions. A possible mechanism of the UVB quenching is also the change of the charge state of the in-plane carbon dimer, that causes a light emission in a different optical range. In addition, *ex-situ* analyzes reveal an important side effect of prolonged electron irradiation, such as the 40 nm thick deposition of tetrahedral amorphous carbon on top of the hBN flake. This is a clear evolution of the well-established electron beam induced surface contamination due to the adsorption of carbonic species.

## 1. Introduction

With the growing interest in quantum optics applications [1–4], hexagonal boron nitride (hBN) has emerged as a promising platform for high-yield, room-temperature single-photon emitters (SPEs) based on color centers [5–10]. The generation and tuning of color centers with SPE properties in hBN can be achieved through various approaches [8, 11–18]. Among these, irradiation with charged particles has shown several advantages [7, 11, 19], including spatial localization [20–22] and the creation of

high-formation-energy point defects, such as the boron vacancy [9, 23–26].

Electron irradiation offers the highest spatial localization of radiative centers [20–22]. The color centers generated by this technique depend on irradiation parameters, with light emissions spanning from blue to infrared by varying factors such as accelerating voltage, beam current, or irradiation time [20–22, 27]. Recently, cathodoluminescence (CL) has facilitated studies of SPE-related color centers in hBN [20, 23, 28–32]. Notably, recent research has demonstrated the potential of CL for *in-situ* monitoring

of localized activation of blue-emitting color centers through spot-mode electron beam irradiation [33, 34]. CL is one of the most versatile experimental tools for studying and monitoring the optical properties of hBN [12, 35–41]. Typically conducted at cryogenic temperatures, CL can excite near-band-edge (NBE) emissions of hBN (5.8 eV, 212 nm) in the deep ultraviolet (UV) region [36, 38]. Furthermore, CL has been used to unambiguously identify hBN crystalline phases [42] and detect UV emission at 300 nm (4.1 eV), which is modulated by the twist angle of stacked hBN multilayers [31, 43]. Finally, CL analysis is important for the CL is also critical for identifying unique optical features in hBN microstructures, such as bubbles and wrinkles [39, 44, 45].

In this study, we present an efficient and rapid procedure involving large-area, fast-scanning, low-voltage electron irradiation to suppress undesired defect-related radiative recombination. This process is monitored via *in-situ* CL hyperspectral analysis. Prolonged irradiation leads to a monotonic quenching of deep-level UV emissions and a concurrent narrowing of NBE UV emissions in hBN. The quenching of the UV band (UVB) is attributed to the electron beam-induced dissociation of in-plane carbon dimers, into different configurations of the donor acceptor pair of substitutional carbon atoms with different spatial separations in the hBN lattice, that can be optically inactive or emits light in a different optical range. An additional mechanism of the UVB quenching is the positively or negatively charging of the in-plane carbon dimer, that would cause a light emission in a different optical range. This hypothesis is supported by the observed decrease in below-bandgap excitation photoluminescence (PL) emissions. *Ex-situ* Raman and atomic force microscopy (AFM) analyzes reveal a notable side effect of prolonged large-area, low-voltage electron irradiation: the deposition of a 40 nm thick layer of tetrahedral amorphous carbon. This outcome highlights the evolution of surface contamination induced by electron beam exposure due to the adsorption of carbonaceous species.

## 2. Results

Figure 1 illustrates the schematic setup of the experiment, which combines CL measurements and electron irradiation, conducted at room temperature. The first step of the experiment is a CL hyperspectral mapping of the hBN flake of interest. Specifically, the mapping is performed using an acceleration voltage of 5 keV and an electron beam current of 150 pA. The hyperspectral map is a  $1024 \times 1024$  array of spectral acquisitions across the selected area, with an acquisition time of 1 s per spectrum. A representative CL spectrum for a 400 nm-thick hBN flake is

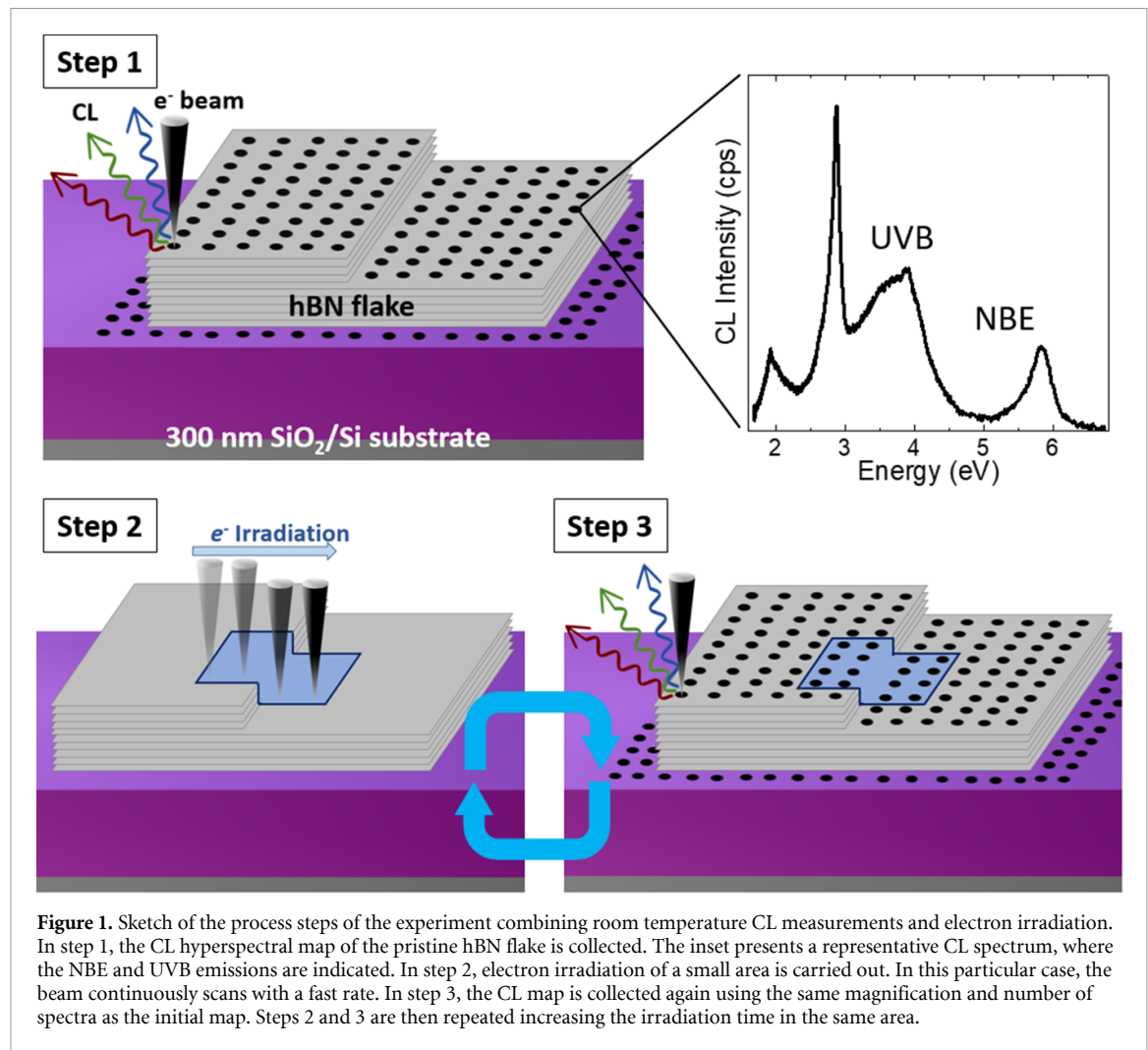
shown in figure 1. The thickness of the hBN flake is precisely measured using AFM, as detailed in figure S1, confirming a thickness of 400 nm. The CL spectrum reveals several light emission peaks: an asymmetric emission at 5.83 eV (212 nm) and a broad band centered at 3.73 eV (332 nm). Additional peaks are set at 2.91 eV (426 nm) and 1.92 eV (646 nm) which are identified as second-order diffraction of the 5.83 eV and 3.73 eV radiative recombination processes.

The sharp peak at 5.83 eV corresponds to the NBE phonon-assisted recombination in hBN at room temperature [46]. This emission arises from s-like free excitons [38, 40, 47]. The low-energy tail of this peak is attributed to the D series, which represents radiative recombination associated with extended structural defects, such as stacking faults [48], dislocations [49] or grain boundaries [47]. The broad emission band at 3.73 eV, commonly referred to as the UVB, is attributed to radiative transitions involving impurities and their phonon replicas [38, 50].

The second step of the experiment involves irradiating the hBN flake, as indicated by the blue square in figure 1. For this step, an accelerating voltage of 5 kV and a beam current of 90 pA are used to irradiate a  $30 \mu\text{m} \times 30 \mu\text{m}$  area. During irradiation, the electron beam scans the area at the maximum available scan rate of 2 MHz per frame, as provided by the scanning electron microscope (SEM). This ensures spatial homogeneity of the irradiation dose. The 5 kV accelerating voltage is selected to maximize the number of scattering events within the hBN flake (as supported by the Monte Carlo simulation shown in figure S2). Additionally, this irradiation condition keeps the system within the dynamic charging regime, enabling valuable secondary electron (SE) imaging [51–54]. Importantly, at low accelerating voltages, the process occurs at energy levels far below the knock-on energy threshold (120 keV) of the hBN lattice atoms [55]. Consequently, the irradiation does not generate new crystalline defects.

The third step of the experiment involves acquiring a CL hyperspectral map of the same area analyzed in Step 1. Steps 2 and 3 are then repeated, consistently involving the same area. The hBN flake is irradiated for a total of 60 min, divided into two sessions: an initial 15 min round, followed by a 45 min round.

The SE imaging of the hBN flake is shown in figure 2(a). When increasing the irradiation time, it is possible to distinguish the exposed area by a local change in the SE contrast. It is worth noting that the 15 min low-voltage irradiation (figure 2(b)) changes the SE contrast homogeneously in the treated area. Increasing the irradiation time to 60 min (figure 2(c)) causes two main effects: the appearance of several bright contrast lines and a charging striping effect in the adjacent area. Using the standard formula for the SE contrast ( $C$ ) of an object, we can perform a more



quantitative analysis of the effect of electron irradiation on the SE contrast [56]:

$$C = \left( \frac{I_{\text{OBJ}} - I_{\text{BG}}}{I_{\text{BG}}} \right) \times 100$$

where  $I_{\text{OBJ}}$  is the average SE intensity of the of the area of interest, and  $I_{\text{BG}}$  is the average SE intensity of the background. The SE contrast of the exposed area increases by 37% after 15 min of irradiation. This enhanced brightness is attributed to negative charging within the irradiated region [51]. After 60 min of irradiation, the SE contrast in the irradiated area is only 16% brighter than the background. This reduced increase in dynamic charging, combined with the presence of a dark frame surrounding the irradiated region and several brighter lines, indicates surface contamination of the hBN, likely caused by the adsorption of carbonaceous species. Additionally, the charge striping effect results in a 65% increase in SE contrast in the adjacent area. The preferential charging observed to the right of the irradiated region is attributed to the beam's scanning direction, which progresses from left to right [53].

The CL spectra of hBN as a function of increasing electron irradiation time are shown in figure 3(a). The primary evolution of the CL lineshape with irradiation time is characterized by a decrease in the intensity of the UVB band. Furthermore, the full width at half maximum (FWHM) of the NBE emission narrows with increasing irradiation time. Specifically, the pristine hBN exhibits an FWHM of 450 meV, which decreases to 420 meV after 15 min of irradiation and reaches a minimum of 360 meV after 60 min. CL integrated intensity and FWHM of the NBE and the second order diffraction bands as function of the irradiation time are reported in figure S3.

The evolution of the integrated CL intensities of the UVB and NBE emissions, along with their intensity ratio as a function of irradiation time, is shown in figure 3(b). The UVB emission is identified as a complex convolution of multiple radiative recombination processes. A detailed deconvolution of the UVB band, presented in figure S4, reveals three distinct components. Two of these bands, located at 4.03 eV and 3.86 eV, are attributed to the zero-phonon line (ZPL) of carbon defects and its corresponding phonon

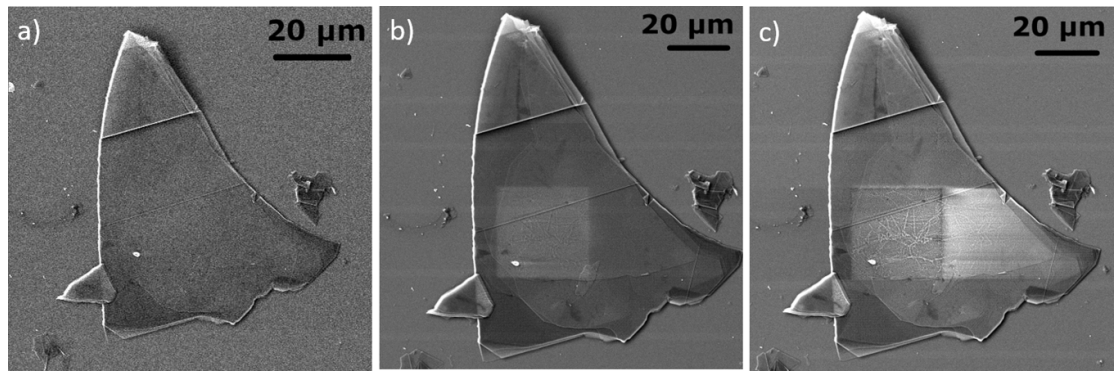


**Figure 2.** SEM micrograph, obtained with an Everhart–Thornley detector, of the analyzed flake before and after each irradiation step: (a) pristine, (b) after 15 min, and (c) after 60 min.

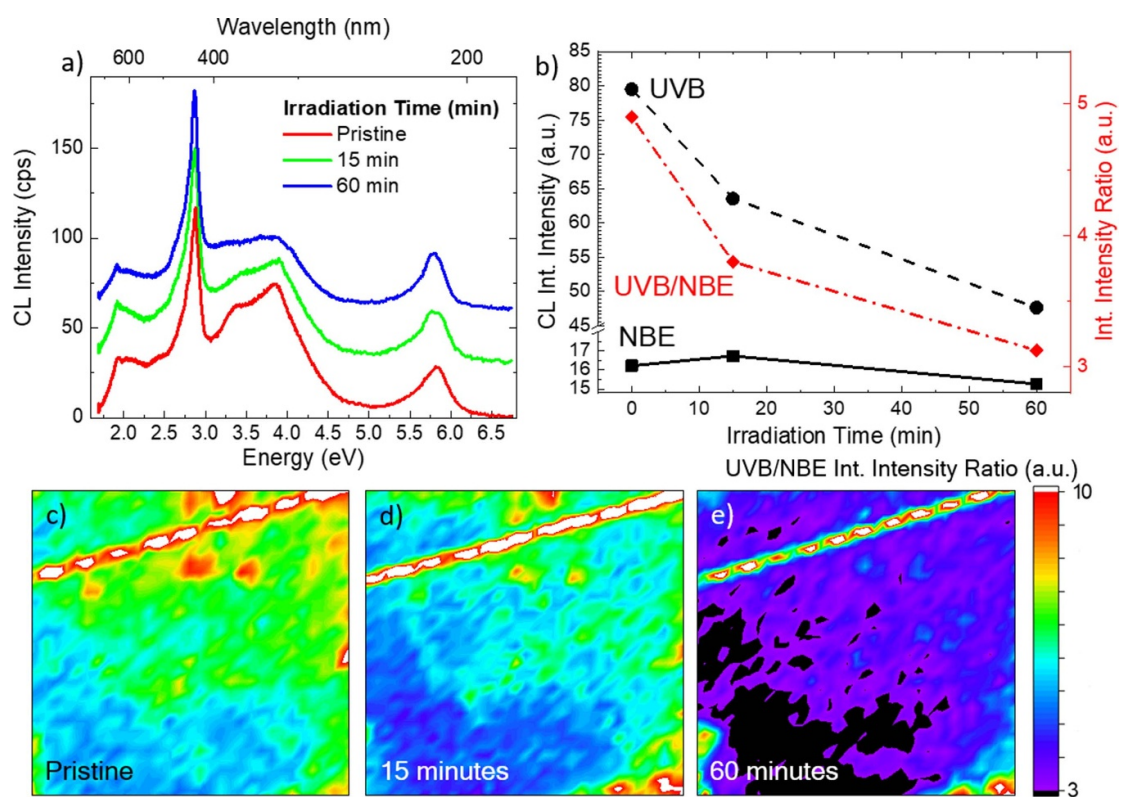
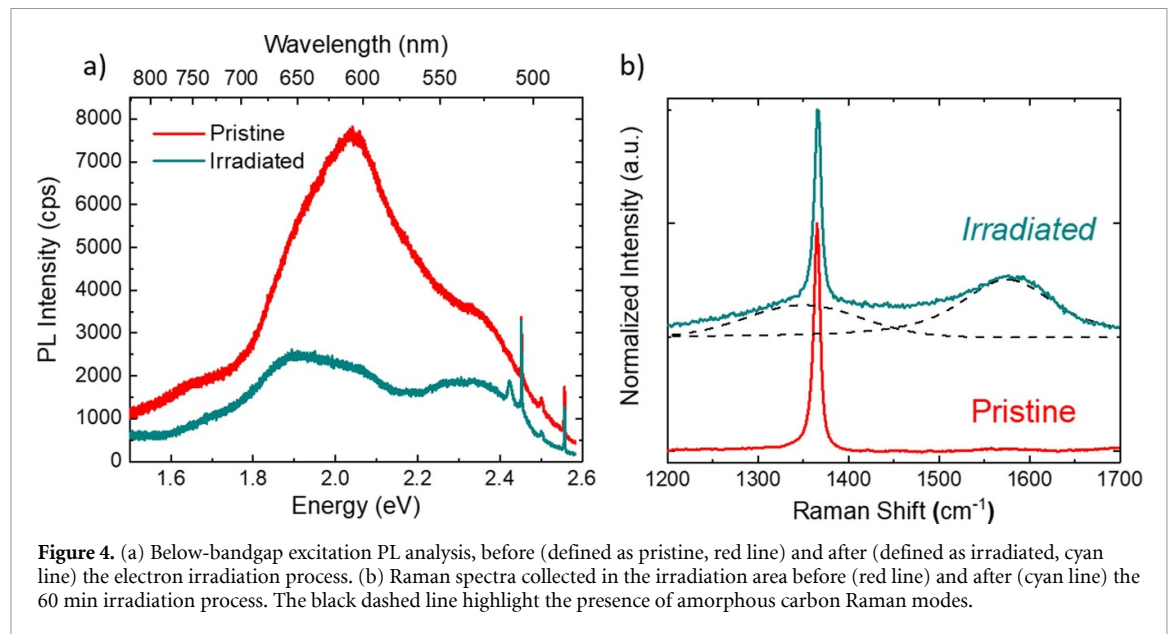


**Figure 3.** (a) Representative CL spectra of the hBN flat area: pristine (red line), after 15 min of irradiation (green line), and after 60 min (blue line). For clarity, the CL spectra are shifted vertically every 30 cps. (b) CL integrated intensity of the UVB (black circles) and NBE (black squares) bands and the UVB/NBE integrated intensity ratio (red symbols) as function of the irradiation time. UVB/NBE integrated intensity ratio maps, acquired in the same area: (c) pristine hBN, (d) of 15 min irradiated and (e) 60 min irradiated, respectively.

replica [57, 58]. An additional emission at 3.43 eV is reported, probably related to a donor–acceptor pair [59]. The integrated intensity of the UVB emission decreases by 20% after 15 min of irradiation and declines by an additional 20% following 60 min of irradiation. In contrast, the integrated intensity of the NBE recombination exhibits a peak after 15 min of irradiation, with an increase of 3.2%. However, this intensity subsequently decreases by 6% after 60 min of irradiation. To illustrate the evolution of UVB

and NBE emission intensities with increasing electron irradiation time, we present the CL mapping of the UVB/NBE integrated intensity ratio for the different irradiation steps in figures 3(c)–(e), respectively. The UVB/NBE ratio is widely recognized as a key indicator of defect density [40, 47]. The intensity ratio is not uniform across the analyzed area, indicating a spatially inhomogeneous distribution of defect density. Nevertheless, the primary effect of electron irradiation is a consistent, homogeneous decrease in





the UVB/NBE integrated intensity ratio over time (figure 3(b)).

To investigate the origin of the UVB band quenching, we performed *ex-situ* optical and structural analyzes. Recent studies have shown that below-bandgap excitation PL analysis can offer valuable insights into the presence of deep levels within the hBN bandgap [44]. Specifically, it has been shown that the PL emission between 1.8 eV and 2.5 eV originates from radiative recombination involving the same deep levels responsible for the CL emission observed between 3.0 eV and 4.5 eV [44]. The PL spectra of the hBN flake before and after the 60 min irradiation process are shown in figure 4(a). Due to the *ex-situ* nature of the investigation, only the PL spectrum of the 60 min irradiated sample is presented. The irradiation process results in a significant decrease in luminescence intensity across the entire energy range. Notably, the PL spectra consist of multiple emissions, with their Gaussian deconvolutions provided in figure S5.

The most prominent effect of the irradiation process is the substantial quenching of the broad emission at 2.03 eV, which decreases by 66%. This quenching is considerably more severe than the intensity reductions observed for the 2.33 eV and 1.88 eV components, which decrease by 44% and 47%, respectively. The below-bandgap excitation PL analysis confirms the irradiation-induced modifications to the deep-level emissions previously identified in the CL analysis, as shown in figure 3.

Raman spectroscopy has been employed to identify possible structural changes in the irradiated area by analyzing the hBN Raman mode FWHM. The Raman peak, which is conventionally investigated in hBN, is at 1365 cm<sup>-1</sup>. This mode is attributed

to the in-plane atom vibrations ( $E_{2g}$  mode) [60]. Figure 4(b) presents the Raman spectra before irradiation (defined as pristine, red line), and after irradiation and exposure to the lab environment (defined as irradiated, cyan line). The careful analysis of the  $E_{2g}$  mode FWHM shows that the irradiation process causes a broadening of the peak from 8.3 cm<sup>-1</sup> to 8.7 cm<sup>-1</sup>. This broadening is an indication of the degradation of the crystalline quality of the hBN lattice. The Raman spectrum after irradiation presents also the appearance of an additional broad bands at 1575 cm<sup>-1</sup> and at 1350 cm<sup>-1</sup> superimposed to the hBN Raman mode. These modifications to the Raman spectrum can be attributed to the surface contamination by hydrocarbon species [61] and the consequent modification of such species by the electron beam irradiation. In fact, the broad mode at 1575 cm<sup>-1</sup> and at 1350 cm<sup>-1</sup> can be assigned to the G and D modes of amorphous carbon. The Raman lineshape can indicate the presence of partially recrystallized tetrahedral amorphous carbon (ta-C) [62, 63]. This attribution is mainly supported by the Raman shift of the G mode at 1575 cm<sup>-1</sup> and the D/G intensity ratio equal to 0.5. In fact, The increase of the D peak intensity in ta-C is due to an increase of the sp<sup>2</sup> bonds cause by electron beam irradiation [64, 65]. In our case, the 60 min electron irradiation process provides enough energy to transform the hydrocarbon contaminants in ta-C and then to enhance the crystallinity of the deposited layer. The Raman intensity maps of the hBN and G modes are reported in figure S5 in order to highlight the spatial localization of the G mode in the irradiated area. An actual trend in the Raman analysis of particles irradiated hBN is reporting a defect activated Raman modes (graphene D peak like) of hBN [66–68]. While the authors of

these works have attributed these Raman modes to defect-activated modes of hBN, our data suggests that these Raman modes appear to be related to the presence of amorphous carbon, deposited during the irradiation processes [7, 21, 69]. The morphological analysis of the irradiated area, carried out by AFM, reveals the presence of a 43 nm thick amorphous carbon layer as reported in figure S7.

### 3. Discussion

The UVB quenching observed in both PL and CL experiments indicates a reduction in the concentration of defects that facilitate radiative recombination within the hBN bandgap. This effect can be attributed to two possible mechanisms: electron beam annealing of the irradiated region of the hBN flake or the electron beam-induced dissociation of defects responsible for the UVB emission. To evaluate the potential for electron beam annealing, we estimated the local temperature increase caused by electron beam irradiation by comparing two well-established models: the modified Vine-Einstein model [70, 71] and the Baker-Sexton model [72]. The temperature increase is estimated to be 85 K using the Vine-Einstein model and 115 K using the Baker-Sexton model. All parameters and formulas used for these temperature estimations are provided in table S1. However, the estimated temperature increase is likely insufficient to modify the radiative defects responsible for the UVB emission. Notably, high-temperature annealing processes ( $T \geq 1273$  K) are typically required to eliminate radiative defects in hBN [73, 74]. Therefore, we attribute the dissociation of defects by the electron beam as the most probable cause of the UVB emission reduction. Similar effects have been reported for low energy electron beam irradiation in C-doped hBN [34], Mg-doped GaN thin film [75, 76], GaN quantum wells [77] and diamond films [78–80]. To clarify the dissociation process occurring during electron irradiation, it is essential to identify the origin of the UVB band. Several studies have attributed the UVB emission to carbon-containing defects [30, 81–85]. In particular, recent works have addressed the in-plane carbon dimer ( $C_B C_N$ ) as the defect originating the 4.1 eV ZPL emission [57, 58, 86–89]. The in-plane carbon dimer has a formation energy of approximately 2 eV [58]. Consequently, the energy delivered by electron beam irradiation (250 eV across the entire thickness of the hBN flake, as shown in figure S2, for a single irradiation event) is sufficient to cause the dissociation of this defect. This energy is delivered through multiple scattering events, that occurs during the long-time irradiation process.

The in-plane carbon dimer dissociation may lead to a different configuration of carbon substitutional centers. The most probable configuration is the

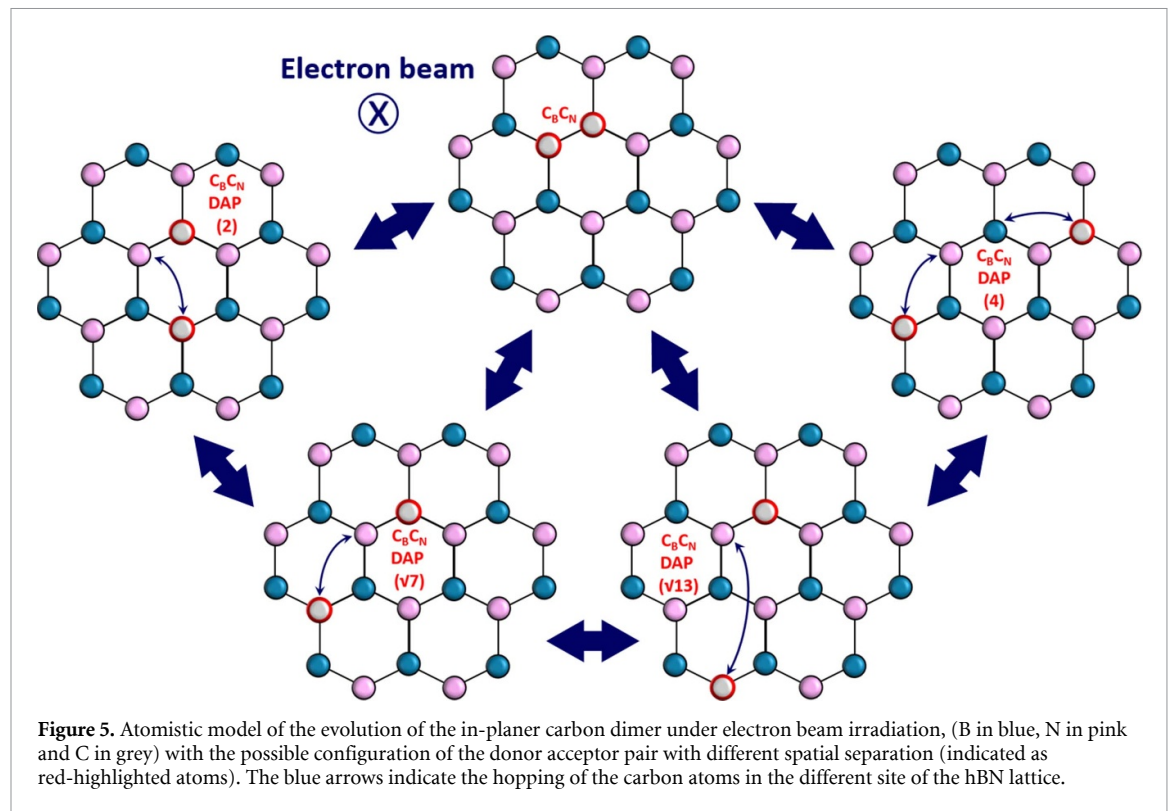
donor–acceptor pair composed of a carbon atom in boron position and in nitrogen position ( $C_B C_N$ -DAP). These configurations are energetically favored, considering the energy provided by the scattering events with the electron beam [86]. These particular configurations present radiative recombination in the range of the second order diffraction of the UVB or outside of the optical range analyzed in this work [86]. The atomistic model of the evolution of the in-plane carbon dimer is presented in figure 5, reporting the possible configuration of the  $C_B C_N$ -DAP with different spatial separation. The calculated ZPL of the different configuration of the ( $C_B C_N$ -DAP) are reported in table S2. A possible change of the charge state of the  $C_B C_N$  center is a possible mechanism for the quenching of the UVB. In fact, the ZPL of the positively and negatively charged carbon dimer falls in an optical range not analyzed in the present work. In particular, the positively charged  $C_B C_N$  is expected to present a light emission at 1.055 eV while the negatively charged one should emit light at 0.442 eV [86]. The SE contrast analysis, reported in figure 2, suggests the negative charge state of the  $C_B C_N$  donor acceptor pair.

The possible rise of amorphous carbon induced artifacts, affecting the *in-situ* CL analysis, is reported in figure S8.

### 4. Conclusions

In conclusion, we demonstrate an efficient and rapid method for suppressing undesired defect-related radiative recombination in hBN through large-area, fast-scanning, low-voltage electron irradiation, monitored via *in-situ* CL hyperspectral analysis. Prolonged irradiation leads to a monotonic quenching of deep-level UV emissions and a concurrent narrowing of NBE UV emissions. The quenching of the UVB is ascribed to the electron beam-induced dissociation of in-plane carbon dimers, into different configurations of the donor acceptor pair of substitutional carbon atoms, that can be optically inactive or emits light in a different optical range. An additional mechanism of the UVB quenching is the change of the charge state of the  $C_B C_N$  center, that causes a light emission in a different optical range. This interpretation is further supported by the observed reduction in *ex-situ* below-bandgap excitation PL emissions.

Additionally, *ex-situ* Raman and AFM analyzes reveal a significant side effect of prolonged electron irradiation: the formation of a 40 nm thick layer of tetrahedral amorphous carbon. This result underscores the evolution of electron beam-induced surface contamination, caused by the adsorption of carbonaceous species, observed by SE contrast modification during the *in-situ* CL analysis.



## 5. Experimental methods

We obtain the hBN flake via standard micro-mechanical exfoliation from bulk single crystals [44, 82].

The CL measurements and sample irradiation processes are carried out in a CL dedicated Attolight Rosa SEM microscope. The specimen is left overnight in vacuum for an effective degassing of the SEM chamber. The electron irradiation is carried out with an accelerating voltage of 5 kV and a beam current of 91 pA, keeping the electron beam scanning over the area of interest at a frequency of 2 MHz/frame. The total dose in the first round of irradiation (15 min) is  $177 \text{ mC cm}^{-2}$  and  $708 \text{ mC cm}^{-2}$  during the 60 min irradiation.

The integrated intensity of the NBE is evaluated between 6.25 eV and 5 eV, while for the UVB emission, the integrated intensity is obtained between 5 eV and 3.2 eV.

The SEM images are taken *in-situ* with a standard Everhart–Thornley detector for SEs. The CL measurements are carried out at room temperature, with an accelerating voltage of 5 kV and a beam current of 150 pA. The CL signal is sent to a spectrometer by means of an objective ( $\text{NA} = 0.71$ ) placed in the electron microscope. The system is equipped with a  $600 \text{ l mm}^{-1}$  diffraction grating and a Peltier-cooled charge-coupled device.

AFM measurements are performed using a Dimension Icon AFM (Bruker) operating in Peak Force mode and using a ScanAsyst probe.

Raman and PL experiments are carried out with a Renishaw InVia system, equipped with a confocal microscope, a 473 nm excitation laser and a 2400 line/mm grating. The Raman measurements are taken with the following parameters: excitation laser power 1 mW, 10 s acquisition time for each spectrum and a spot size of 800 nm (100X objective with  $\text{NA} = 0.85$ ). The PL experiments are carried out with the same parameters, except for an acquisition of 30 s.

## Data availability statement

The data that support the findings of this study are openly available at the following URL/DOI: <https://10.5281/zenodo.14671078>.

## Acknowledgment

F F wants to thank C Blaga, N Tappy and Professor A Fontcuberta i Morral for the scientific discussions. F B, S P and F F thank Dr C Coletti from the Istituto Italiano di Tecnologia for the access to the micro-Raman facility. K W and T T acknowledge support from the JSPS KAKENHI (Grant Numbers 21H05233 and 23H02052), the CREST (JPMJCR24A5), JST



and World Premier International Research Center Initiative (WPI), MEXT, Japan.

## Conflict of interest

The authors declare no conflict of interest.

## Contributions

K.W. and T.T. provided the hBN crystals. S.P. exfoliated the hBN flakes. F.B. carried out the micro-Raman and PL spectroscopies measurements. F.F. carried out the *in-situ* CL spectroscopic measurements and the AFM analysis. F. F. and F. B. analyzed and interpreted the data. F.F. conceived the idea of the experiment, coordinated research efforts and wrote the paper. All authors participated in reviewing the manuscript.

## ORCID iDs

F Bianco  <https://orcid.org/0000-0002-6372-8889>

S Pezzini  <https://orcid.org/0000-0003-4289-907X>

K Watanabe  <https://orcid.org/0000-0003-3701-8119>

F Fabbri  <https://orcid.org/0000-0003-1142-0441>

## References

- [1] Caldwell J D, Aharonovich I, Cassabois G, Edgar J H, Gil B and Basov D N 2019 Photonics with hexagonal boron nitride *Nat. Rev. Mater.* **4** 552–67
- [2] Turunen M, Brotons-Gisbert M, Dai Y, Wang Y, Scerri E, Bonato C, Jöns K D, Sun Z and Gerardot B D 2022 Quantum photonics with layered 2D materials *Nat. Rev. Phys.* **4** 219–236
- [3] Moon S, Kim J, Park J, Im S, Kim J, Hwang I and Kim J K 2023 Hexagonal boron nitride for next-generation photonics and electronics *Adv. Mater.* **35** 2204161
- [4] Kim S, Frösch J E, Christian J, Straw M, Bishop J, Totonjian D, Watanabe K, Taniguchi T, Toth M and Aharonovich I 2018 Photonic crystal cavities from hexagonal boron nitride *Nat. Commun.* **9** 2623
- [5] Fernandes J, Queirós T, Rodrigues J, Nemala S S, LaGrow A P, Placidi E, Alpuim P, Nieder J B and Capasso A 2022 Room-temperature emitters in wafer-scale few-layer hBN by atmospheric pressure CVD *FlatChem* **33** 100366
- [6] Gan L, Zhang D, Zhang R, Zhang Q, Sun H, Li Y and Ning C-Z 2022 Large-scale, high-yield laser fabrication of bright and pure single-photon emitters at room temperature in hexagonal boron nitride *ACS Nano* **16** 14254–61
- [7] Grosso G, Moon H, Lienhard B, Ali S, Efetov D K, Furchi M M, Jarillo-Herrero P, Ford M J, Aharonovich I and Englund D 2017 Tunable and high-purity room temperature single-photon emission from atomic defects in hexagonal boron nitride *Nat. Commun.* **8** 705
- [8] Tran T T, Elbadawi C, Totonjian D, Lobo C J, Grosso G, Moon H, Englund D R, Ford M J, Aharonovich I and Toth M 2016 Robust multicolor single photon emission from point defects in hexagonal boron nitride *ACS Nano* **10** 7331–8
- [9] Gottscholl A *et al* 2020 Initialization and read-out of intrinsic spin defects in a van der Waals crystal at room temperature *Nat. Mater.* **19** 540–5
- [10] Kianinia M, Regan B, Tawfik S A, Tran T T, Ford M J, Aharonovich I and Toth M 2017 Robust solid-state quantum system operating at 800 K *ACS Photonics* **4** 768–73
- [11] Fischer M *et al* 2024 Controlled generation of luminescent centers in hexagonal boron nitride by irradiation engineering *Sci. Adv.* **7** eabe7138
- [12] Mendelson N *et al* 2021 Identifying carbon as the source of visible single-photon emission from hexagonal boron nitride *Nat. Mater.* **20** 321–8
- [13] Liu G-L *et al* 2023 Single photon emitters in hexagonal boron nitride fabricated by focused helium ion beam *Adv. Opt. Mater.* **12** 2302083
- [14] Sajid A, Ford M J and Reimers J R 2020 Single-photon emitters in hexagonal boron nitride: a review of progress *Rep. Prog. Phys.* **83** 44501
- [15] Xu Z-Q *et al* 2018 Single photon emission from plasma treated 2D hexagonal boron nitride *Nanoscale* **10** 7957–65
- [16] Choi S, Tran T T, Elbadawi C, Lobo C, Wang X, Juodkazis S, Seniutinas G, Toth M and Aharonovich I 2016 Engineering and localization of quantum emitters in large hexagonal boron nitride layers *ACS Appl. Mater. Interfaces* **8** 29642–8
- [17] Kozawa D *et al* 2023 Discretized hexagonal boron nitride quantum emitters and their chemical interconversion *Nanotechnology* **34** 115702
- [18] Ronceray N *et al* 2023 Liquid-activated quantum emission from pristine hexagonal boron nitride for nanofluidic sensing *Nat. Mater.* **22** 1236–42
- [19] Ngoc My Duong H, Nguyen M A P, Kianinia M, Ohshima T, Abe H, Watanabe K, Taniguchi T, Edgar J H, Aharonovich I and Toth M 2018 Effects of high-energy electron irradiation on quantum emitters in hexagonal boron nitride *ACS Appl. Mater. Interfaces* **10** 24886–91
- [20] Gale A, Li C, Chen Y, Watanabe K, Taniguchi T, Aharonovich I and Toth M 2022 Site-specific fabrication of blue quantum emitters in hexagonal boron nitride *ACS Photonics* **9** 2170–7
- [21] Bianco F, Corte E, Ditalia Tchernij S, Forneris J and Fabbri F 2023 Engineering multicolor radiative centers in hBN flakes by varying the electron beam irradiation parameters *Nanomaterials* **13** 739
- [22] Fournier C *et al* 2021 Position-controlled quantum emitters with reproducible emission wavelength in hexagonal boron nitride *Nat. Commun.* **12** 3779
- [23] Sarkar S, Xu Y, Mathew S, Lal M, Chung J-Y, Lee H Y, Watanabe K, Taniguchi T, Venkatesan T and Gradečak S 2024 Identifying luminescent boron vacancies in h-BN generated using controlled He<sup>+</sup> Ion irradiation *Nano Lett.* **24** 43–50
- [24] Zabelotsky T *et al* 2023 Creation of boron vacancies in hexagonal boron nitride exfoliated from bulk crystals for quantum sensing *ACS Appl. Nano Mater.* **6** 21671–8
- [25] Whitefield B, Toth M, Aharonovich I, Tetienne J-P and Kianinia M 2023 Magnetic field sensitivity optimization of negatively charged boron vacancy defects in hBN *Adv. Quantum Technol.* **n/a** 2300118
- [26] Glushkov E *et al* 2022 Engineering optically active defects in hexagonal boron nitride using focused ion beam and water *ACS Nano* **16** 3695–703
- [27] Kumar A, Cholsuk C, Zand A, Mishuk M N, Matthes T, Eilenberger F, Suwanna S and Vogl T 2023 Localized creation of yellow single photon emitting carbon complexes in hexagonal boron nitride *APL Mater.* **11** 71108
- [28] Chen X, Yue X, Zhang L, Xu X, Liu F, Feng M, Hu Z, Yan Y, Scheuer J and Fu X 2023 Exotic single-photon and enhanced deep-level emissions in hBN strain superlattice (arXiv:2302.07614)
- [29] Hayee F *et al* 2020 Revealing multiple classes of stable quantum emitters in hexagonal boron nitride with correlated optical and electron microscopy *Nat. Mater.* **19** 534–9
- [30] Bourrellier R, Meuret S, Tararan A, Stéphan O, Kociak M, Tizei L H G and Zobelli A 2016 Bright UV single photon emission at point defects in h-BN *Nano Lett.* **16** 4317–21
- [31] Lee H Y, Al Ezzi M M, Raghuvanshi N, Chung J Y, Watanabe K, Taniguchi T, Garaj S, Adam S and Gradečak S 2021 Tunable optical properties of thin films controlled by the interface twist angle *Nano Lett.* **21** 2832–9

- [32] Chen X, Yue X, Zhang L, Xu X, Liu F, Feng M, Hu Z, Yan Y, Scheuer J and Fu X 2024 Activated single photon emitters and enhanced deep-level emissions in hexagonal boron nitride strain crystal *Adv. Funct. Mater.* **34** 2306128
- [33] Roux S, Fournier C, Watanabe K, Taniguchi T, Hermier J-P, Barjon J and Delteil A 2022 Cathodoluminescence monitoring of quantum emitter activation in hexagonal boron nitride *Appl. Phys. Lett.* **121** 184002
- [34] Nedić S, Yamamura K, Gale A, Aharonovich I and Toth M 2024 Electron beam restructuring of quantum emitters in hexagonal boron nitride *Adv. Optical Mater.* **12** 2400908
- [35] Shima K, Cheng T S, Mellor C J, Beton P H, Elias C, Valvin P, Gil B, Cassaboies G, Novikov S V and Chichibu S F 2024 Cathodoluminescence spectroscopy of monolayer hexagonal boron nitride *Sci. Rep.* **14** 169
- [36] Kubota Y, Watanabe K, Tsuda O and Taniguchi T 2007 Deep ultraviolet light-emitting hexagonal boron nitride synthesized at atmospheric pressure *Science* **317** 932–4
- [37] López-Morales G I et al 2021 Investigation of photon emitters in Ce-implanted hexagonal boron nitride *Opt. Mater. Express* **11** 3478–85
- [38] Watanabe K, Taniguchi T and Kanda H 2004 Direct-bandgap properties and evidence for ultraviolet lasing of hexagonal boron nitride single crystal *Nat. Mater.* **3** 404–9
- [39] Curie D et al 2022 Correlative nanoscale imaging of strained hBN spin defects *ACS Appl. Mater. Interfaces* **14** 41361–8
- [40] Schué L, Stenger I, Fossard F, Loiseau A and Barjon J 2016 Characterization methods dedicated to nanometer-thick hBN layers *2D Mater.* **4** 15028
- [41] Maestre C et al 2022 From the synthesis of hBN crystals to their use as nanosheets in van der Waals heterostructures *2D Mater.* **9** 35008
- [42] Zanfrognini M et al 2023 Distinguishing different stackings in layered materials via luminescence spectroscopy *Phys. Rev. Lett.* **131** 206902
- [43] Su C et al 2022 Tuning colour centres at a twisted hexagonal boron nitride interface *Nat. Mater.* **21** 896–902
- [44] Ciampalini G, Blaga C V, Tappy N, Pezzini S, Watanabe K, Taniguchi T, Bianco F, Roddaro S, Fontcuberta I Morral A and Fabbri F 2022 Light emission properties of mechanical exfoliation induced extended defects in hexagonal boron nitride flakes *2D Mater.* **9** 35018
- [45] Lee H Y, Sarkar S, Reidy K, Kumar A, Klein J, Watanabe K, Taniguchi T, LeBeau J M, Ross F M and Gradečak S 2022 Strong and localized luminescence from interface bubbles between stacked hBN multilayers *Nat. Commun.* **13** 5000
- [46] Valvin P, Pelini T, Cassaboies G, Zobelli A, Li J, Edgar J H and Gil B 2020 Deep ultraviolet hyperspectral cryomicroscopy in boron nitride: photoluminescence in crystals with an ultra-low defect density *AIP Adv.* **10** 75025
- [47] Pierret A, Loayza J, Berini B, Betz A, Plaçais B, Ducastelle F, Barjon J and Loiseau A 2014 Excitonic recombinations in h-BN: from bulk to exfoliated layers *Phys. Rev. B* **89** 35414
- [48] Watanabe K, Taniguchi T, Kuroda T and Kanda H 2006 Effects of deformation on band-edge luminescence of hexagonal boron nitride single crystals *Appl. Phys. Lett.* **89** 141902
- [49] Jaffrennou P, Barjon J, Lauret J-S, Attal-Trétout B, Ducastelle F and Loiseau A 2007 Origin of the excitonic recombinations in hexagonal boron nitride by spatially resolved cathodoluminescence spectroscopy *J. Appl. Phys.* **102** 116102
- [50] Museur L, Feldbach E and Kanaev A 2008 Defect-related photoluminescence of hexagonal boron nitride *Phys. Rev. B* **78** 155204
- [51] Joy D C and Joy C S 1995 Dynamic charging in the low voltage SEM *Microsc. Microanal.* **1** 109–12
- [52] Joy D C 1989 Control of charging in low-voltage SEM *Scanning* **11** 1–4
- [53] Cazaux J 2004 Charging in scanning electron microscopy “from inside and outside” *Scanning* **26** 181–203
- [54] Joy D C and Joy C S 1996 Low voltage scanning electron microscopy *Micron* **27** 247–63
- [55] Kotakoski J, Jin C H, Lehtinen O, Suenaga K and Krasheninnikov A V 2010 Electron knock-on damage in hexagonal boron nitride monolayers *Phys. Rev. B* **82** 113404
- [56] Reimer L 2000 Scanning electron microscopy: physics of image formation and microanalysis *Meas. Sci. Technol.* **11** 1826
- [57] Plo J, Pershin A, Li S, Poirier T, Janzen E, Schutte H, Tian M, Wynn M, Bernard S and Rousseau A 2024 Isotope substitution and polytype control for point defects identification: the case of the ultraviolet color center in hexagonal boron nitride (arXiv:2405.20837)
- [58] Mackoīt-Sinkevičienė M, Maciaszek M, Van de Walle C G and Alkauskas A 2019 Carbon dimer defect as a source of the 4.1 eV luminescence in hexagonal boron nitride *Appl. Phys. Lett.* **115** 212101
- [59] Zhang S, Li K, Guo C and Ping Y 2023 Effect of environmental screening and strain on optoelectronic properties of two-dimensional quantum defects *2D Mater.* **10** 35036
- [60] Geick R, Perry C H and Rupprecht G 1966 Normal modes in hexagonal boron nitride *Phys. Rev.* **146** 543–7
- [61] Yagodkin D et al 2022 Extrinsic localized excitons in patterned 2D semiconductors *Adv. Funct. Mater.* **32** 2203060
- [62] Ferrari A C and Robertson J 2000 Interpretation of Raman spectra of disordered and amorphous carbon *Phys. Rev. B* **61** 14095–107
- [63] Ferrari A C, Kleinsorge B, Morrison N A, Hart A, Stolojan V and Robertson J 1999 Stress reduction and bond stability during thermal annealing of tetrahedral amorphous carbon *J. Appl. Phys.* **85** 7191–7
- [64] Klein F, Treske U, Koitzsch A, Cavicchia D R, Thönnissen C, Frömter R, Roch T and Mühl T 2016 Nanoscale scanning electron microscopy based graphitization in tetrahedral amorphous carbon thin films *Carbon* **107** 536–41
- [65] Yajima A, Abe S, Fuse T, Mera Y, Maeda K and Suzuki K 2002 Electron-irradiation-induced ordering in tetrahedral-amorphous carbon films *Mol. Cryst. Liq. Cryst.* **388** 147–51
- [66] Liang H et al 2022 High sensitivity spin defects in hBN Created by high-energy He beam irradiation *Adv. Opt. Mater.* **11** 2201941
- [67] Gu R et al 2021 Engineering and microscopic mechanism of quantum emitters induced by heavy Ions in hBN *ACS Photonics* **2912–22**
- [68] Venturi G, Chiodini S, Melchioni N, Janzen E, Edgar J H, Ronning C and Ambrosio A 2024 Selective generation of luminescent defects in hexagonal boron nitride *Laser Photonics Rev.* **18** 2300973
- [69] Nanda G, Goswami S, Watanabe K, Taniguchi T and Alkemade P F A 2015 Defect control and n-doping of encapsulated graphene by helium-ion-beam irradiation *Nano Lett.* **15** 4006–12
- [70] Myhajlenko S, Ke W and Hamilton B 1983 Cathodoluminescence assessment of electron beam recrystallized silicon *J. Appl. Phys.* **54** 862–7
- [71] Yacobi B G and Holt D B 1986 Cathodoluminescence scanning electron microscopy of semiconductors *J. Appl. Phys.* **59** R1–24
- [72] Baker B G and Sexton B A 1975 Electron beam effects in auger analysis of physisorbed xenon *Surf. Sci.* **52** 353–64
- [73] Chen Y, Gale A, Yamamura K, Horder J, Condos A, Watanabe K, Taniguchi T, Toth M and Aharonovich I 2023 Annealing of blue quantum emitters in carbon-doped hexagonal boron nitride *Appl. Phys. Lett.* **123** 41902
- [74] Ren F, Wu Y and Xu Z 2023 Creation and repair of luminescence defects in hexagonal boron nitride by irradiation and annealing for optical neutron detection *J. Lumin.* **261** 119911
- [75] Gelhausen O, Klein H N, Phillips M R and Goldys E M 2002 Influence of low-energy electron beam irradiation on defects in activated Mg-doped GaN *Appl. Phys. Lett.* **81** 3747–9

- [76] Gelhausen O, Klein H N, Phillips M R and Goldys E M 2003 Low-energy electron-beam irradiation and yellow luminescence in activated Mg-doped GaN *Appl. Phys. Lett.* **83** 3293–5
- [77] Jahn U, Dhar S, Kostial H, Watson I M and Fujiwara K 2003 Low-energy electron-beam irradiation of GaN-based quantum well structures *Phys. Status Solidi c* **2223–6**
- [78] Zachreson C, Martin A A, Aharonovich I and Toth M 2014 Electron beam controlled restructuring of luminescence centers in polycrystalline diamond *ACS Appl. Mater. Interfaces* **6** 10367–72
- [79] Barjon J, Chevallier J, Jomard F, Baron C and Deneuville A 2006 Electron-beam-induced dissociation of B–D complexes in diamond *Appl. Phys. Lett.* **89** 232111
- [80] Won J H, Hatta A, Yagyu H, Ito T, Sasaki T and Hiraki A 1996 Dependence of cathodoluminescence on irradiation time in diamond *Phys. Status Solidi* **154** 321–6
- [81] Du X Z, Li J, Lin J Y and Jiang H X 2015 The origin of deep-level impurity transitions in hexagonal boron nitride *Appl. Phys. Lett.* **106** 21110
- [82] Taniguchi T and Watanabe K 2007 Synthesis of high-purity boron nitride single crystals under high pressure by using Ba–BN solvent *J. Cryst. Growth* **303** 525–9
- [83] Li S, Pershin A, Thiering G, Udvarhelyi P and Gali A 2022 Ultraviolet quantum emitters in hexagonal boron nitride from carbon clusters *J. Phys. Chem. Lett.* **13** 3150–7
- [84] Wang G, Cheng Y, Chen J, Meng J, Zeng L, Yin Z, Wu J and Zhang X 2023 Luminescence properties of the hexagonal boron nitride epilayer *Adv. Opt. Mater.* **11** 2301034
- [85] Onodera M, Isayama M, Taniguchi T, Watanabe K, Masubuchi S, Moriya R, Haga T, Fujimoto Y, Saito S and Machida T 2020 Carbon annealed HPHT-hexagonal boron nitride: exploring defect levels using 2D materials combined through van der Waals interface *Carbon* **167** 785–91
- [86] Auburger P and Gali A 2021 Towards ab initio identification of paramagnetic substitutional carbon defects in hexagonal boron nitride acting as quantum bits *Phys. Rev. B* **104** 75410
- [87] Winter M, Bousquet M H E, Jacquemin D, Duchemin I and Blase X 2021 Photoluminescent properties of the carbon-dimer defect in hexagonal boron-nitride: a many-body finite-size cluster approach *Phys. Rev. Mater.* **5** 95201
- [88] Jara C, Rauch T, Botti S, Marques M A L, Norambuena A, Coto R, Castellanos-Águila J E, Maze J R and Munoz F 2021 First-principles identification of single photon emitters based on carbon clusters in hexagonal boron nitride *J. Phys. Chem. A* **125** 1325–35
- [89] Pelini T *et al* 2019 Shallow and deep levels in carbon-doped hexagonal boron nitride crystals *Phys. Rev. Mater.* **3** 94001